HHS Public Access

Author manuscript

Nat Methods. Author manuscript; available in PMC 2012 November 01.

Published in final edited form as:

Nat Methods. ; 9(5): 477–479. doi:10.1038/nmeth.1945.

Direct visualization of specifically modified extracellular glycans in living animals

Matthew Attreed[1], **Muriel Desbois**[1], **Toin H. van Kuppevelt**[2], and **Hannes E. Bülow**[1,3,*]

[1]Department of Genetics, Albert Einstein College of Medicine, Bronx, New York, USA
[2]Department of Biochemistry, Radboud University Nijmegen Medical Centre Nijmegen Centre for Molecular Life Sciences (NCMLS), Nijmegen, Netherlands [3]Dominick P. Purpura Department of Neuroscience, Albert Einstein College of Medicine, Bronx, New York, USA

Abstract

Modification patterns of the extracellular glycan heparan sulfate coordinate protein function in metazoans, yet *in vivo* imaging of such non-genetically encoded structures has been impossible. Here we report a transgenic method in *Caenorhabditis elegans* that allows direct live imaging of specific heparan sulfate modification patterns. This experimental approach reveals a dynamic and cell-specific heparan sulfate landscape and could in principle be adapted to visualize and analyze any extracellular molecule *in vivo*.

Fluorescent protein fusions [1] allow live imaging of virtually every protein. In contrast, *in vivo* visualization of non-genetically encoded molecules such as glycans or lipids is more challenging. Using 'click' chemistry some glycans have been visualized in live zebrafish and *Caenorhabditis elegans* [2,3], but modifications of the glycans, which are crucial for the function of many molecules, cannot be distinguished. For example, heparan sulfates are extracellular glycosaminoglycans with complex modification patterns (Fig. 1a) that are attached to heparan sulfate proteoglycan core proteins such as membrane associated syndecans, glypicans, or the secreted perlecan and agrin [4,5]. Heparan sulfate modification patterns play pivotal roles in metazoan development and physiology by interacting with, and modulating the function of a wide array of proteins [4,5]. Biochemical studies and the identification of specific neuroanatomical defects of mutants in heparan sulfate genes in vertebrates and invertebrates have led to the "Heparan sulfate code" hypothesis which posits that distinct heparan sulfate modification patterns are localized in a tissue- or cell-specific pattern, particularly in the nervous system [6].

We developed an *in vivo* technique to visualize and analyze complex heparan sulfate modification patterns to directly test this hypothesis. To this end, we made use of a subset of

*corresponding author: Telephone 718 430 3621, Fax 718 430 8778, hannes.buelow@einstein.yu.edu.

Author contributions

M.A. conducted all experiments. M.D. constructed several transgenic strains and important constructs. T.v.K. contributed vsv-tagged scFv antibody preparations. M.A. and H.E.B. analyzed data and wrote the manuscript with editorial input from M.D. and T.v.K..

heparan sulfate-specific single chain variable fragment (scFv) antibodies [7] that recognize specifically modified forms of HS (Table 1). We fused a secretion signal and green fluorescent protein (GFP) to the N-terminus and C-terminus of heparan sulfate-specific scFv antibodies, respectively and expressed these constructs in six scavenger cells (coelomocytes) in *C. elegans* (Fig. 1b, Supplementary Fig. 1). Focusing initially on the HS4C3 scFv antibody [8] we found that transgenic expression of a secreted *HS4C3::GFP* fusion produced discrete staining *in vivo*, predominantly in the nervous system (Fig. 1c-o). We did not observe similar staining patterns in animals expressing a negative control antibody fusion (*MPB49::GFP)* that differs from the HS4C3 antibody in merely five amino acids and has no known epitope (Fig. 1h, Table 1)[9]. Staining patterns appeared independent of the promoter used to express the scFv-antibody fusion (Supplementary Fig. 2), the fluorescent protein (Supplementary Fig. 3) or the level of transgene expression (Supplementary Fig. 4). Lastly, the stained structures in the nervous system are distant from the site of antibody expression and secretion from the coelomocytes. The *in vivo* staining patterns of transgenic antibodies were overlapping but not identical to immunohistochemical stains of fixed animals which in addition to the nervous system and pharynx included the intestine (Supplementary Fig. 5). This suggests that some heparan sulfate may be located in cellular compartments that were inaccessible to the secreted transgenic scFv antibody *GFP* fusions. We conclude that the observed staining patterns are specific for the *HS4C3::GFP* antibody fusion.

In vitro, the scFv HS4C3 recognizes an HS epitope comprising 3-*O*-sulfated and 6-*O*-sulfated glucosamine residues with a minor contribution of 2-*O*-sulfation on hexuronic acid moieties [8]. To determine whether the transgenically expressed *HS4C3::GFP* antibody fusion recognized heparan sulfate with similar specificity we removed genes required for heparan sulfate modifications and quantified relative fluorescence, using the prominent nerve ring staining as a proxy (Supplementary Fig. 6a). Genetic removal of the heparan sulfate 6-*O*-sulfotransferase *hst-6* or both 3-*O*-sulfotransferases reduced nerve ring staining (Fig. 1i,**l**,**p**), whereas individual removal of the 3O-sulfotransferases *hst-3.1* or *hst-3.2* resulted in no reduction of nerve ring staining (Fig. 1j,**k**,**p**). This suggested that *hst-3.1* and *hst-3.2* can act redundantly in forming the heparan sulfate modification pattern recognized by the *HS4C3::GFP* antibody fusion. In contrast, genetic removal of the heparan sulfate *C*-5 epimerase *hse-5* or 2-*O*-sulfotransferase *hst-2* increased nerve ring staining (Fig. 1m,**n**,**p**). Since *hst-2* restricts heparan sulfate 6-*O*-sulfation [10], its removal increased 6-*O*-sulfation which may be sufficient for increased binding or, alternatively, 2-*O*-sulfation may have an inhibitory effect on binding of the *HS4C3::GFP* antibody fusion. We found nerve ring staining in the *hst-6 hst-2* double mutant significantly reduced compared to the *hst-6* single mutant ($P = 1.25 \times 10^{-7}$, $n = 34$, Fig. 1i,**o**,**p**), demonstrating that (1) increased staining in *hst-2* mutants was *hst-6* dependent and (2) that in the absence of *hst-6*, nerve ring staining was dependent on, rather than being inhibited by, the 2-*O*-sulfotransferase *hst-2* and by inference 2-*O*-sulfation..

We next tested which HS core protein(s) bears the heparan sulfate epitope recognized by the *HS4C3::GFP* antibody fusion. Removal of the single *C. elegans sdn-1*/syndecan, but not the two glypicans (*gpn-1, lon-2*), perlecan (*unc-52*), or agrin eliminated staining of the nerve ring as well as nerve cords, indicating that the majority of heparan sulfate recognized by the

HS4C3::GFP antibody fusion is associated with the nervous system and attached to the syndecan core protein (Fig. 1q, Supplementary Fig. 6b-g). Increased nerve ring staining upon loss of *gpn-1*/glypican was *sdn-1*/syndecan-dependent (Fig. 1q, Supplementary Fig. 6b,c,f), possibly due to compensatory mechanisms. Interestingly, staining of structures outside of the nerve ring was reduced in strains lacking *sdn*-1/syndecan (Supplementary Fig. 6c,f), consistent with the interpretation that *HS4C3::GFP* recognized heparan sulfate epitopes attached to *sdn*-1/syndecan with possibly lower affinity. The differences in staining in heparan sulfate mutants were neither due to changes in transgene expression (Supplementary Fig. 7), nor the permeability of basement membranes as a result of an altered charge distribution [11]. First, the distribution of the *MPB49::GFP* control antibody fusion was unaffected in heparan sulfate mutant backgrounds (Supplementary Fig. 8) and second, different heparan sulfate-specific antibody *GFP* fusions displayed distinct specificities compared to the *HS4C3::GFP* antibody fusion (Table 1, Supplementary Fig. 9). Thus, the *HS4C3::GFP* fusion recognizes a heparan sulfate modification pattern *in vivo* that is borne by the syndecan core protein, and consistent with *in vitro* binding studies of HS4C3 [8], involves 6-*O*-, 3-*O*- and 2-*O*-sulfation for optimal binding.

To study the dynamics and diversity of heparan sulfate modification patterns *in vivo*, we analyzed animals expressing *HS4C3::GFP* and several additional heparan sulfate-specific scFv-antibody fusions with different binding characteristics, including *HS3A8::GFP*, *AO4B08::GFP*, and *EW3G6::GFP* (Table 1, Supplementary Fig. 9). The *HS4C3::GFP* antibody fusion was associated specifically with the nervous system from the embryonic 3-fold stage through larval into adult stages (Fig. 2a-c,**g**, Supplementary Fig. 10). The nerve ring which forms the major neuropil in the worm appeared diffusely stained, whereas staining of the dorsal and ventral nerve cords appeared more punctate and of approximately equal intensity (Fig. 2g). Thus, heparan sulfate may be associated with motor neuron processes which are present in roughly equal numbers in the dorsal and ventral cords. During later larval stages, we observed discrete staining of the vulval epithelium and uterine tissues (Fig. 2f). By late larval and adult stages, we detected additional staining of the basement membranes that surround the body wall muscles (Fig. 2c,**e**,**k**) and the anterior and posterior bulbs of the pharynx (Fig. 2g). We do not know whether as a secreted molecule heparan sulfate is expressed by the stained tissues or produced non-autonomously by surrounding tissues.

We found staining by the *HS3A8::GFP* fusion to be very similar, yet stronger than *HS4C3::GFP* (Fig. 2h). Since *in vivo* binding characteristics of HS3A8 and HS4C3 were distinct (Table 1, Supplementary Fig. 9) and both antibody fusions showed incomplete overlap in colocalization studies (Supplementary Fig. 11), we suggest that HS4C3 recognizes a heparan sulfate modification pattern that partially overlaps with the epitope recognized by HS3A8. Similarly, the *AO4B08::GFP* fusion labeled the nerve ring and the nerve cords in a both overlapping and distinct fashion. The nerve ring displayed more discrete, sheath-like staining in close apposition to the pharynx, rather than the diffuse staining seen with the *HS4C3::GFP* fusion (Fig. 2i). This staining could be associated with the sheath-like extensions of the GLR cells or the muscle plate that wraps around the pharynx [12]. Intriguingly, the *EW3G6::GFP* fusion did not label body wall muscles at all.

Rather, *EW3G6::GFP* appeared to stain exclusively part of the neurites but not cell bodies of a single pair of neurons. This suggests the existence of unique and cell-specific heparan sulfate modification patterns that are localized to defined subcellular structures (Fig. 2j). We also detected differences in staining outside of the nervous system (Fig. 2i, Supplementary Figure 12). We conclude that individual cells can express cell-specific heparan sulfate modification patterns that are associated with defined subcellular-specific structures and dynamically remodeled during development.

Whereas the *C. elegans* system can take advantage of coelomocytes to remove unbound antibody fusions, transgenic approaches in other genetic models could use inducible systems to limit antibody production. The transgenic expression of scFv antibody GFP fusions shares several unique features. First, while shown here for heparan sulfate, this approach should in principle be applicable to live imaging of any molecule such as glycans or lipids, as well as proteins undergoing posttranslational modification through phosphorylation, sulfation, acetylation or glycosylation as long as specific scFv antibodies exist. Second, it renders non-genetically encoded molecules amenable to genetic analysis to probe their biosynthesis and, possibly, function. While we do not observe obvious defects in transgenic worms, our method could conceivably combine visualization with functional interference if the antibody fragment had the ability to functionally neutralize its epitope, as has been shown in cell culture experiments [13]. Last, it should allow to study the dynamics of such molecules *in vivo*, including live 4D imaging of remodeling and, possibly, turnover.. Our technique potentially allows development of *in vivo* biosensors for essentially any molecule and would expand the toolbox for *in vivo* visualization and analysis of molecules in living animals.

Online Methods

Strains

Worms were cultured as previously described [17]. The following strains and alleles were used: N2 Bristol wild-type, *hse-5(tm472)* (OH1487), *hst-2(ok595)* (OH1876), *hst-6(ok273)* (OH1421), *hst-3.1(tm734)* (EB649), *hst-3.2(tm3006)* (EB650), sdn-1(zh20), gpn-1(ok377), lon-2(e678), unc-52(e998), agr-1(tm2051), unc-104(rh43), otIs76 mgIs18 (OH904), dzEx195 [Punc-122::HS4C3::GFP(S65T); rol-6(su1006)] (EB313), dzEx341 [Punc-122::HS3A8::GFP(S65T); rol-6(su1006)] (EB569), dzEx369 [Punc-122::AO4B08::GFP(S65T); rol-6(su1006)] (EB637), *dzEx475 [Punc-122::EW3G6::2xsfGFP; rol-6(su1006)]* (EB917), dzEx206 [Punc-122::MPB49::GFP(S65T); rol-6(su1006)] (EB324), dzIs10V [Punc-122::HS4C3::GFP(S65T); rol-6(su1006)] (EB502), *dzIs13 [Punc-122::HS3A8::GFP(S65T); rol-6(su1006)]* (EB667), dzIs14 [Punc-122::AO4B08::GFP(S65T); rol-6(su1006)] (EB668), *dzIs16 [Punc:: 122::MPB49::GFP(S65T)]* (EB703), *otIs173III [Prgef-1::DsRed2; Pttx-3::GFP]* [18]. Doubles between heparan sulfate mutant strains and antibody expressing strains were constructed using standard procedures. Details for genotyping are available on request.

To create transgenic worms, single chain variable fragment (scFv) antibody constructs were injected with *pRF4* (*rol-6(su1006)*) as a dominant injection marker at 25 ng/μl and 100 ng/μl, respectively. Several transgenic lines giving comparable results were obtained for

each construct. The transgenic lines *dzEx195*, *dzEx341*, *dzEx369*, and *dzEx206* were integrated to yield *dzIs10V*, *dzIs13*, *dzIs14*, and *dzIs16*, respectively. All mutants and integrated transgenes were backcrossed at least four times prior to analysis.

scFv::GFP antibody fusion constructs

A panel of scFv antibodies that bind different heparan sulfate preparations were originally isolated from a phage display library [19]. The antibodies comprise different variable heavy chains as indicated (Table 1) and an invariant variable light chain [19]. To assemble the transgenic antibody expression constructs, we used the following general scheme. Sequences of the invariable light chain and each published variable heavy chain were optimized for *C. elegans* codon usage and synthesized *de novo* by Entelechon (Regensburg, Germany). The scFv heavy chains were then assembled with the invariable light chain using a set of unique restriction sites (Supplementary Fig. 1). Subsequently, the scFv antibodies were cloned SalI/AgeI into *pJF33* [*Pmyo-3::secGFP(S65T)*] [20] to yield a fusion protein in which the scFv antibody is N-terminally fused in frame to the SEL-1 signal sequence [21] and C-terminally to the S65T green fluorescent protein variant (Supplementary Fig. 1). scFv constructs sharing the same heavy chain but differing in the CDR3 region (EW3G6 and HS3A8) were built by PCR mediated mutagenesis using a Quickchange kit (Stratagene) using the following primers
TATTATTGTGCCAGAGGAGGAACCACCCGCATCCGCAAGTGGGGACAGGGAAC A and
TGTTCCCTGTCCCCACTTGCGGATGCGGGTGGTTCCTCCTCTGGCACAATAATA (for EW3G6) and,
TATTATTGTGCCAGAGGAATGCGTCCACGCCTTTGGGGACAGGGAACA and TGTTCCCTGTCCCCAAAGGCGTGGACGCATTCCTCTGGCACAATAATA (for HS3A8). The completed scFv antibody cassettes were subcloned under the control of the coelomocyte-specific *unc-122* promoter [22] or *glo-1* promoter [23]. The *EW3G6* scFv was fused with two consecutive sfGFP (superfolder GFP) molecules (2xsfGFP) using an established PCR fusion technique [24] and cloned under control of the *unc-122* promoter. All sequences that were synthesized *de novo* or underwent PCR amplification were verified by sequencing and are available upon request.

Fluorometric and microscopic analyses

For quantitative epifluorescence microscopy, worms were synchronized by hypochlorite bleaching and plated on regular nematode plates with OP50 *E. coli*. Approximately 24h later, animals were washed off in M9, anaesthetized with 1mM levamisole, mounted on a 5% agarose pad and analyzed on an AxioImagerZ1 compound microscope (Zeiss) or a Leica SP2 AOBS confocal microscope. All images used for quantification were taken with an exposure time of 250 ms at 400× magnification and fluorimetrically analyzed using Zeiss AxioVision software version 4.8 as follows. Relative pixel intensity in a region of “specific fluorescence” around the nerve ring was measured and divided by the relative pixel intensity measured in a region of “total fluorescence” comprising the whole head to the posterior end of the pharynx (Supplementary Fig. 6) to yield relative fluorescence. Care was taken to exclude fluorescing coelomocytes from this quantification, although this was not possible in a few select cases due to coelomocyte migration defects (e.g. some *sdn-1* mutants animals).

Since this did not obviously affect total head fluorescence (Supplementary Fig. 7) which serves as the denominator, we included these values in the calculations of relative fluorescence. Statistical significance was calculated using the two-tailed Student's t-test with the Bonferroni correction where applicable.

Microscopic images were acquired with an AxioCam MRm camera mounted on an AxioImager Z1 compound microscope using Axiovision 4.8 Zeiss proprietary software. For preparation of figures we exported images from Axiovision 4.8 by applying a 5% bestfit gamma curve. Some animals were optically sectioned using the Zeiss Apotome on an AxioImager Z1 or a Leica SP2 AOBS confocal microscope. Optical sections were processed as 12-bit grayscale images using Zeiss Axiovision software 4.8 (if obtained with the Apotome) or as 8-bit grayscale images using ImageJ (if obtained with the Leica confocal) to produce maximum intensity projections. All images were assembled into figures using Adobe Photoshop and Adobe Illustrator.

Supplementary Material

Refer to Web version on PubMed Central for supplementary material.

Acknowledgements

We thank J. Attonito, N. Gomez, and P. Weinberg for technical assistance. We thank H. Fares (University of Arizona, Tucson) for providing the *pJF33* plasmid, E. Snapp (Albert Einstein College of Medicine, Bronx) for the superfolder GFP, and S. Mitani (Tokyo Women's Medical University School of Medicine) for providing the *tm734*, *tm3006*, and *tm3208* alleles of HS 3O-sulfotransferases. We thank L. Attreed, S. Emmons, O. Hobert, and members of the Bülow lab for comments on the manuscript. This work was supported in part by grants from the National Institutes of Health (5R01HD055380 and RC1GM090825 to H.E.B.; T32 GM007491 to M.A.). H.E.B. is an Alfred P. Sloan Fellow.

References

1. Wang S, Hazelrigg T. Nature. 1994; 369:400–03. [PubMed: 7910952]
2. Laughlin ST, Baskin JM, Amacher SL, Bertozzi CR. Science. 2008; 320:664–7. [PubMed: 18451302]
3. Laughlin ST, Bertozzi CR. ACS Chem Biol. 2009; 4:1068–72. [PubMed: 19954190]
4. Bishop JR, Schuksz M, Esko JD. Nature. 2007; 446:1030–7. [PubMed: 17460664]
5. Bülow HE, Hobert O. Ann. Rev. Cell. Dev. Biol. 2006; 22:375–407. [PubMed: 16805665]
6. Holt CE, Dickson BJ. Neuron. 2005; 46:169–72. [PubMed: 15848796]
7. van Kuppevelt TH, Dennissen MA, van Venrooij WJ, Hoet RM, Veerkamp JH. J Biol Chem. 1998; 273:12960–6. [PubMed: 9582329]
8. Ten Dam GB, et al. J Biol Chem. 2006; 281:4654–62. [PubMed: 16373349]
9. Smits NC, et al. Methods Enzymol. 2006; 416:61–87. [PubMed: 17113860]
10. Townley RA, Bülow HE. J Biol Chem. 2011; 286:16824–31. [PubMed: 21454666]
11. Lieleg O, Baumgärtel RM, Bausch AR. Biophys J. 2009; 97:1569–77. [PubMed: 19751661]
12. Hall, DH.; Altun, ZF. C. elegans Atlas. Cold Spring Harbor Laboratory Press; Cold Spring Harbor, New York: 2008. Muscle System; p. 145-188.
13. Jenniskens GJ, et al. FASEB J. 2003; 17:878–80. [PubMed: 12626439]
14. Dennissen MA, et al. J Biol Chem. 2002; 277:10982–6. [PubMed: 11790764]
15. Kurup S, et al. J Biol Chem. 2007; 282:21032–42. [PubMed: 17517889]
16. van de Westerlo EM, et al. Blood. 2002; 99:2427–33. [PubMed: 11895775]
17. Brenner S. Genetics. 1974; 77:71–94. [PubMed: 4366476]

18. Bénard C, Tjoe N, Boulin T, Recio J, Hobert O. Genetics. 2009; 183:917–27. [PubMed: 19737747]
19. van Kuppevelt TH, Dennissen MA, van Venrooij WJ, Hoet RM, Veerkamp JH. J Biol Chem. 1998; 273:12960–6. [PubMed: 9582329]
20. Fares H, Greenwald I. Genetics. 2001; 159:133–45. [PubMed: 11560892]
21. Grant B, Greenwald I. Development. 1997; 124:637–44. [PubMed: 9043078]
22. Loria PM, Hodgkin J, Hobert O. J Neurosci. 2004; 24:2191–201. [PubMed: 14999070]
23. Hermann GJ, et al. Mol Biol Cell. 2005; 16:3273–88. [PubMed: 15843430]
24. Hobert O. Biotechniques. 2002; 32:728–30. [PubMed: 11962590]

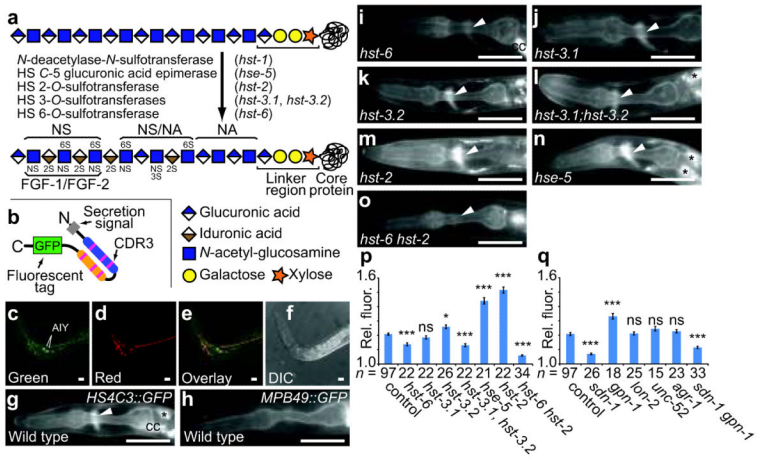

Figure 1. A technique to visualize specifically modified heparan sulfate *in vivo*

(a) Heparan sulfate biosynthesis(NS: *N*-sulfated, NA: *N*-acetylated; 2S, 3S, 6S: 2-*O*-, 3-*O*-, 6-*O*-sulfate; *C. elegans* gene names in parenthesis) and putative protein interacting regions (FGF: fibroblast growth factor). (**b**) Schematic of a transgenic (scFv) antibody-*GFP* fusion comprising an N-terminal secretion signal and a C-terminal green fluorescent protein, with the variable heavy chain and light chains in blue and orange, and the complementarity determining regions (CDR) in magenta.. Confocal (c, **d**, **e**) and differential interference contrast (**f**, DIC) images showing colocalization of a cytoplasmic pan-neuronal red fluorescent marker (*otIs173*) with green *HS4C3::GFP*. AIY interneurons are labeled by a cytoplasmic GFP reporter transgene. (**g**)-(**o**) Heads of L1 animals transgenically expressing the *HS4C3::GFP* fusion under control of the coelomocyte-specific *unc-122* promoter in different mutant backgrounds as indicated. Anterior and dorsal is to the left and top, respectively. An arrowhead indicates the nerve ring region and an asterisk autofluorescence. Scale bar: 25 μm. cc: coelomocyte. (**p**)-(**q**) Quantification of relative nerve ring fluorescence in mutants as indicated. Error bars denote the s. e. m. and statistical significance is indicated: ns, not significant; * $P < 0.05$; *** $P < 0.0005$.

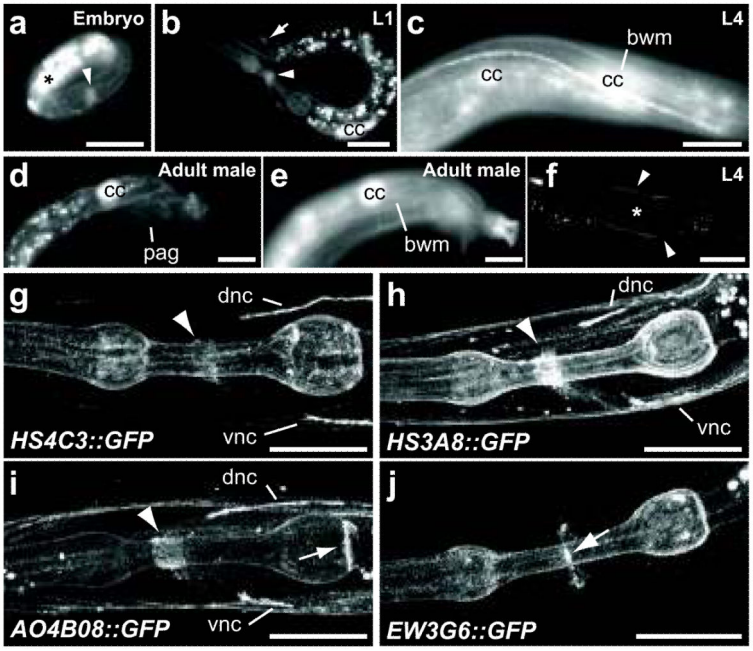

Figure 2. Distinct subcellular HS modification patterns

(**a**) Embryo at 3-fold stage expressing the *HS4C3::GFP* fusion construct. Anterior is to the left in all panels and white arrowheads point to the nerve ring (**a**, **b**, **g-i**) or the vulval epithelium and uterine cells (**f**). Arrows indicate the junction between the pharynx and the intestine (**i**) or the neurites of possibly an individual pair of cells (**j**). A black asterisk denotes gut autofluorescence and a white asterisk the vulva. Scale bar: 25 μm. bwm: body wall muscles, cc: coelomocytes, dnc: dorsal nerve cord, pag: preanal ganglion, and vnc: ventral nerve cord. (**b**) L1 larval stage and (**c**) L4 larval stage animals expressing the *HS4C3::GFP* fusion construct. (**d**)-(**e**) Medial (**d**) and a left, more superficial focal plane (**e**) of a tail of a young adult male displaying staining associated with the preanal ganglion and the intestinal basement membranes (**d**) and body wall muscles (**e**). (**f**) Ventral view showing staining of the vulval epithelium, uterine and possibly cells of the somatic gonad in L4 larval animals expressing the *HS4C3::GFP* fusion. (**g**)-(**j**) Maximum intensity projection of the head of a wild type L4 animal transgenically expressing scFv antibody-GFP fusions as indicated.

Table 1

HS binding characteristics of scFv antibodies *in vitro* and *in vivo*

scFv AB	heavy chain	CDR3 [a]	*in vitro* modifications [b]	*in vivo* modifications [c]
HS4C3 [9]	DP-38	GRRLKD	6S, 3S, (2S)	6S, 3S, (2S)
HS3A8 [14]	DP-38	GMRPRL	6S, 2S, IdoA [14]	6S, 2S
AO4B08 [14]	DP-47	SLRMNGWRAHQ	NS, 6S, 2S, IdoA [15]	6S, 2S
EW3G6 [16]	DP-38	GGTTRIRK	nd	nd
MPB49 [9]	DP-38	WRNDRQ	na	na

[a] Abbreviations: CDR3: variable heavy chain complementarity determining region 3; 6S: HS 6-*O*-sulfate; 3S: HS 3-*O*-sulfate; 2S: HS 2-*O*-sulfate; NS: HS *N*-sulfate, IdoA: iduronic acid as a result of HS *C*-5 glucuronyl-epimerization of glucuronic acid; nd: not determined; na: not applicable.

[b] HS modifications required for optimal competition in ELISAs with major and (minor) contributions.

[c] HS modifications required for binding as determined in this study. Note that in all cases the recognized HS epitopes *in vivo* were attached to the HS core protein syndecan, at least within the nerve ring.